An experimental study of columnar crystals using monodisperse microbubbles.

A. J. Meagher*[a,d], F. García-Moreno[a,b], J. Banhart[a,b], A. Mughal[c] and S. Hutzler[d]

[a] *Technische Universität Berlin, Hardenbergstrasse 36, 10623 Berlin, Germany*
[b] *Institute of Applied Materials, Helmholtz Centre Berlin for Materials and Energy, Hahn-Meitner-Platz 1, 14109 Berlin, Germany.*
[c] *Institute of Mathematics and Physics, Aberystwyth University, Penglais, Aberystwyth, Ceredigion, Wales, SY23 3BZ, United Kingdom*
[d] *School of Physics, Trinity College Dublin, Dublin 2, Ireland*

December 3, 2014

Abstract

We investigate the ordered arrangements of monodisperse microbubbles confined within narrow cylinders. These foams were imaged using X-ray tomography, allowing the 3D positions of the bubbles of the foam to be accurately determined. The structure of these foams closely resemble the minimum energy configuration of hard spheres in cylindrical confinement as found in simulations. For larger ratios, λ, of cylinder to bubble diameter two- and three-layered crystals were formed. Each layer of these structures is found to be ordered, with each internal layer resembling structures found at lower λ values. The average number of contacts per bubble is seen to increase with λ.

1 Introduction

Finding the densest packing of hard spheres is an enduring mathematical problem that finds numerous applications in physics, biology and material sciences. The recent proof of the Kepler conjecture represents a significant milestone in understanding the packing of such objects in an unbounded volume[1]. In contrast, far less is known about packing within a bounded space, despite the fact that such problems are ubiquitous throughout science, nature and even daily life.

*Email:meagheaj@tcd.ie; Fax:004431428611

A fascinating example of this type of problem is that of finding the densest packing of equal sized spheres (of diameter d) in a cylinder (of internal diameter D). Simulations conducted by us (and others) have so far identified some 40 distinct spiral structures in the range $1< \frac{D}{d} <2.873$ - the majority of which are chiral (with achiral packings arising at particular values of $\frac{D}{d}$) [2, 3, 4]. These structures were identified using *simulated annealing*, a numerical technique which can find the minimum energy configuration of a system [3]. Previously, we have dubbed these helical structures columnar crystals and given a theoretical understanding of some of them [3].

Interest in these columnar crystal is driven by the fact that they are chiral and that the degree of chirality depends directly on the ratio $\frac{D}{d}$. Consequently, such structures might find numerous opto-electronic applications, as guides to understanding helical formations in biology (e.g. tobacco virus, flagella and microtubules), or as promising pathways to mimic such biological microstructures [5].

In the range $1< \frac{D}{d} <2.715$ one observes monolayer arrangements (in which all the spheres are in contact with the confining cylinder) while for larger values of $\frac{D}{d}$ we observe more complex multilayer structures that include internal spheres (i.e. spheres which are in contact with other spheres but not in contact with the cylinder). Finding dense hard sphere packings for large values of $\frac{D}{d}$ is a computationally demanding task and as such multilayer arrangements remain largely unexplored [3]. In this paper we show that micron-sized spherical bubbles can spontaneously self-assemble into crystalline arrangements inside capillary tubes, which closely resemble multilayer columnar crystals. We show that by using this method we are able to gain significant insight into the nature of high $\frac{D}{d}$ packings.

Using a microfluidic flow-focusing device we generate wet foams comprised of equal volume bubbles. The bubbles in such foams may be considered spherical since they reside within the *wet region*, H_w, defined as $H_w = \frac{l_0^2}{d}$ where l_0 is the capillary length of the liquid and d is the bubble diameter of the foam [6][1]. Such bubbles have been previously shown to readily assume the minimum-energy configuration of hard-spheres for a wide variety of boundary conditions imposed upon them [7]. By introducing the foam into tubes of different diameters we are able to rapidly generate a variety of helical bubble assemblies. We may classify such structures by the ratio $\lambda = \frac{D}{d}$ where d is the equivalent sphere diameter of the bubbles and D is, again, the diameter of the tube into which the bubbles are placed.

By means of X-ray tomography we are able to access precise 3D information for individual bubbles and obtain the coordination numbers. The resulting foam packings are then compared to the hard-sphere simulations of Pickett and Mughal [2, 3, 4].

2 Experimental method

Monodisperse foam was produced using a flow-focusing device, capable of producing equal-sized bubbles of diameter between 100 μm and 800 μm through

[1] l_0 is defined as $l_0 = \sqrt{\frac{\gamma}{\rho g}}$ where γ is the surface tension, ρ is the density and g is acceleration due to gravity

the controlled co-flow of liquid and gas [8, 9, 10]. The dispersity of bubble diameters of such samples is less than 5%, classifying these foams as monodisperse [11]. In our experiments, we used an aqueous solution composed of 5% by volume commercial detergent *Fairy Liquid* in water. We foamed using Nitrogen gas into which the low-soluble compound perfluorohexane was dissolved. This significantly reduces the coarsening rate of the foam, providing the sample stability required during the imaging of the sample [12].

The bubbles container was fabricated using an *Object Eden 3D* printer composed of a polymer block (24 mm x 24 mm x 40 mm) in which 26 separate cylindrical chambers were formed. The cylinders ranged in diameter from 0.8 mm to 3.3 mm in 0.1 mm intervals. Each cylinder was 18 mm in length. This allows 26 cylindrical packings of different λ values to be imaged at the same time. By repeating the experiment several times with monodisperse foams of different bubble diameters, the variety of different λ-values imaged may be again increased.

The container was placed into a basin of our surfactant solution at the bottom of which was attached a flow-focusing device. The container holding the bubbles was inverted and tapped to remove trapped air, before being again inverted and placed, open face down, over the outlet of the flow-focusing device which had been previously adjusted to produce bubbles of the desired diameter. The container was closed by sliding a glass plate over the open bottom face. The resulting system was then mounted on a polyurethane plinth and allowed to rest for two hours before being imaged. This resting period was found necessary as several bubble re-arrangements were seen to occur just after foam formation. Such movements during the image capture phase would have produced blurring in the final tomographic reconstructions.

Our tomographic device was composed of a micro-focus 150 kV Hamamatsu X-ray source with tungsten target. The sample was mounted on a precision rotation stage from Huber Germany and the sample's radioscopic projections recorded using a flat panel detector C7942 aldo from Hamamatsu(120 mm x 120 mm, 2240 x 2368 pixels, pixel size 50 μm). By varying the filament voltage and current, a 100 kV filament voltage and a 100 μA were found to provide the best contrast and lowest noise in the reconstructed foam images at high spatial resolution for our experimental setup.

The tomographic images were reconstructed using the commercially available software *Octopus* [13]. The data was then analysed using the software package *MAVI* which allowed such information as bubble volume, diameter and position to be extracted [14]. Visualisation of the samples was also performed using the ray-tracing software *povray* which allows for the visual characteristics of individual bubbles to be adjusted [15]. Such software enabled the simultaneous processing and visualisation of the data; the bubbles are eventually represented by spheres of equivalent radius which may then be compared to the results of simulated annealing.

3 Results and discussion

The reconstruction of one of the samples in Fig.1 shows foams formed in cylinders of diameter 2.9 mm, 3 mm, 3.1 mm, 3.2 mm and 3.3 mm (left to right). Each bubble on the exterior of the foam sample may be resolved. As the dis-

tance from the foam-liquid interface increases, the bubbles are seen to become more polyhedral in nature, due to gravitational drainage reducing the liquid fraction of the foam [6].

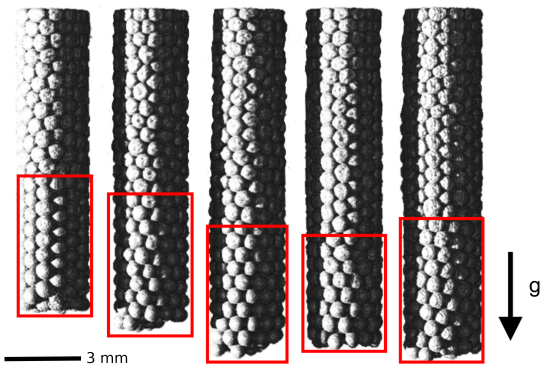

Figure 1: Reconstruction of the raw three-dimensional tomographic data showing the cylindrical ordering of microbubbles. The red boxes indicate regions of consistent ordering. Above these regions, the bubble ordering is seen to change. g shows the direction of gravity.

It can also be seen that the structure of the foam changes as the distance from the foam-liquid interface increases. Specifically, along the vertical axis of the foam in Fig.1, the ordering of the bubbles is seen to change as the distance from the foam-liquid interface is increased. The structures at the top of the foam, far from the foam-liquid interface, have a low liquid fraction and resemble those structures previously reported by Tobin *et. al* [16]. In particular, a series of boundaries is seen to occur. For each crystal, a distinct region of crystallisation near the foam-liquid interface has been highlighted in red allowing the change in ordering to be easily seen. This transition is due to in the gradient of liquid fraction along the length of the foam, resulting in the bubbles becoming more deformed as the distance from the foam-liquid interface is increased, resulting in a change of foam structure. This behaviour may also be thought of as the effect of the buoyancy force of underlying foam layers which leads to an increasing compression of the bubbles in the upwards direction. The results in a reduction in the average separation between bubble centres, creating an apparent reduction in the 'effective' radius of the bubbles within the packing as a function of height, producing crystalline structures associated with higher $\frac{D}{d}$ values at increased distances from the foam-liquid interface.

For comparison with the results of simulated annealing, we wish to examine those wet bubble structures for which the effects of compression are minimal. For this reason, only those bubbles which resided within the capillary length of the surfactant solution $l_0 \approx 1.8$ mm are considered.

3.1 Visual inspection of foam structures

For low-λ values the resulting foam structures are well described by the predictions of simulated annealing. Fig.2 shows the comparison between two foam structures and their hard-sphere counterparts of similar λ values, specifically $\lambda = 2.22 \pm 0.01$ and $\lambda = 2.24 \pm 0.01$. For the structure at λ=2.22, the foam is composed of pairs of bubbles, each layer of bubbles is rotated along the long axis of the foam through 90° with respect to the layer below. The bubbles of each second layer of bubbles are not in contact. Such arrangements are also seen in the hard-sphere simulations. When λ is increased to 2.24, the separation between every second pair of spheres is reduced so that these spheres now touch in both simulation and experiment.

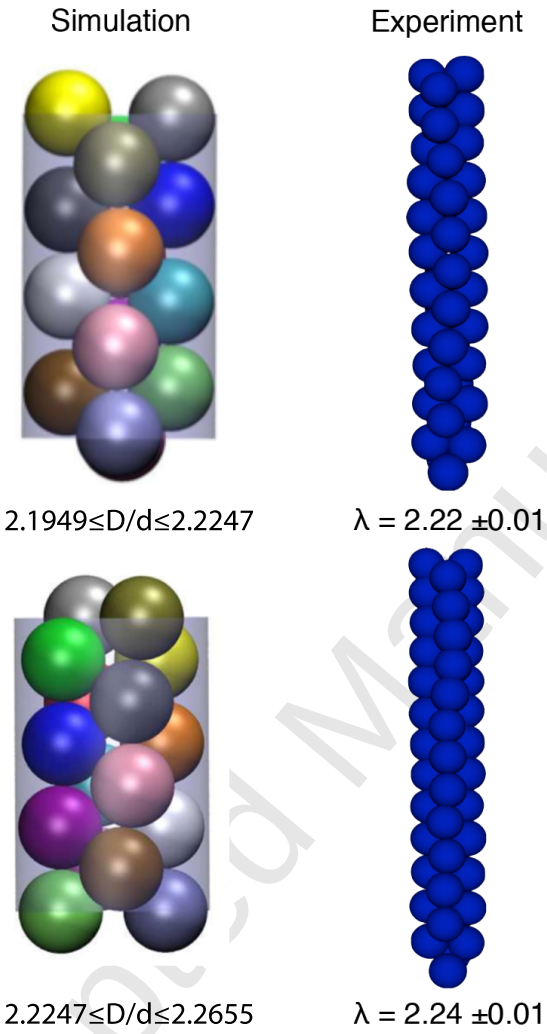

Figure 2: Comparison between the hard-sphere structures produced by simulated annealing (left) and a representation of the foam experiments using visual software *povray* (right). Note that the same arrangement of spheres is seen in both simulation and experiment. The spheres from successive layers or shells are see to touch in both simulation and experiment for $\lambda = 2.22$ and are separated for $\lambda = 2.24$. Data for simulated annealing provided by Mughal *et. al.* [3]

As λ increases the situation is more complicated due to the formation of two- structures with internal spheres. An accurate determination of the exact onset of this transition is not possible from these tomographic experiments due to the inability to continuously measure the structural changes with increasing λ. However, we see that structures without internal spheres form up to $\lambda = 2.5$ while the next successfully imaged structure, at $\lambda = 2.9$, shows the emergence of such spheres. This range of λ values includes $\lambda = 2.73$, the value associated

with the first occurrence of internal spheres in simulation [3].

Several examples of these two-layered structures are shown in Fig.3. Note that a clear distinction exists between internal and external bubbles. In all cases the external bubble layer and internal core are composed of ordered arrangements of bubbles. The internal core of these higher λ value structures resembles structures which appear at lower values of λ. This is clearly seen for $\lambda = 3.4 \pm 0.1$ and $\lambda = 3.6 \pm 0.1$ whose internal structures resemble the zig-zag pattern seen in computational results for $1 < D/d < 1.866$ [4]. On increasing λ, the internal structure again appears to move through a series of structures similar to those reported for lower λ. In Fig.3 the $\lambda = 4.1 \pm 0.1$ structure exhibits an internal core very similar to the simulated structure seen at $D/d = 2.215$.

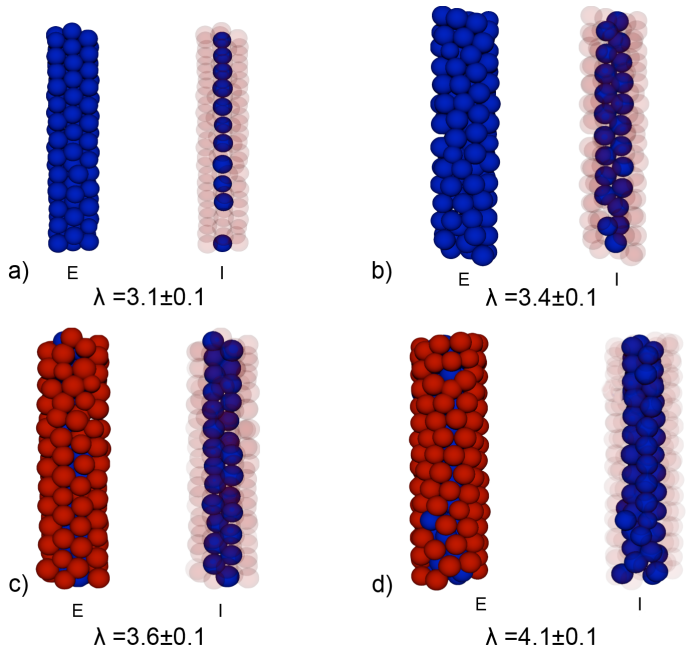

Figure 3: Visualisation of experimental foams of (a) $\lambda = 3.1 \pm 0.1$, (b) $\lambda = 3.4 \pm 0.1$, (c) $\lambda = 3.6 \pm 0.1$ and (d) $\lambda = 4.1 \pm 0.1$ showing (E) the external and (I) the internal structure.

On further increasing the λ value of the foam structures a third layer of ordered bubbles occurs, examples of which are seen in Fig.4. Again each layer appears to be ordered, with each internal layer resembling structures which appear at lower λ values. In the examples we have shown here, increasing the λ value of the structures results in the bubbles of the inner core coming closer together. From the behaviour of doubled-layered structures at lower λ values, we suspect that further increase in λ may result in the formation of a zig-zag structure, as seen for the two-layered structures previously discussed.

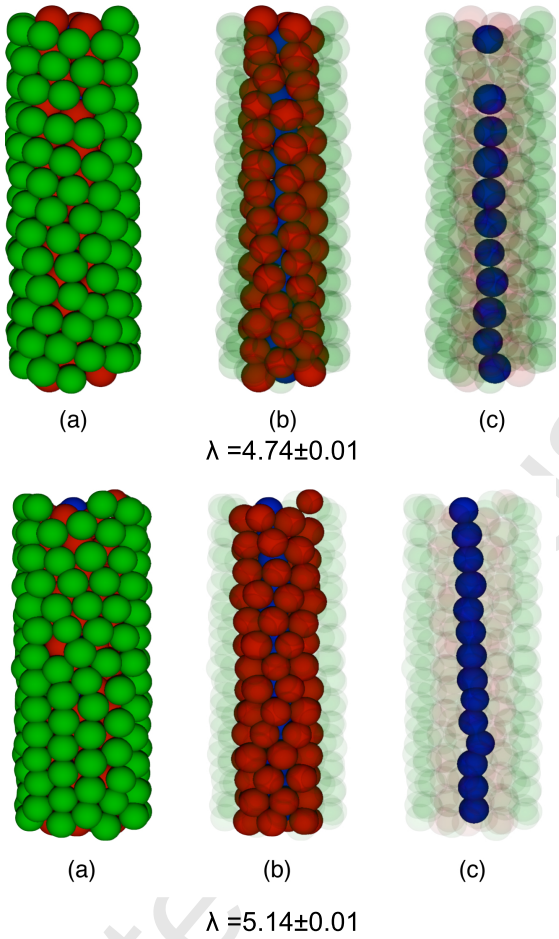

Figure 4: Visualisation of the foam packing structure for $\lambda = 4.74 \pm 0.01$ and $\lambda = 5.14 \pm 0.01$. Successive radially ordered shells of the foam sample are coloured green, red and blue. Each successive layer of the foam is seen to be ordered

3.2 Variation of average contact number

The contact number distribution contact number distribution of the number of neighbours of each bubble within the system - was calculated for each experimental cylindrical packing. Two bubbles are considered neighbours if

$$|\vec{x}_i - \vec{x}_j| \leq R_i + R_j \tag{1}$$

where $\vec{x}_i$ and $\vec{x}_j$ are the centre positions of the i^{th} and j^{th} bubbles within the system and R_i and R_j are the bubble radii. After excluding those bubbles in contact with the foam-liquid interface, the variation of the average number of contacts C with λ was plotted, as shown in Fig.5.

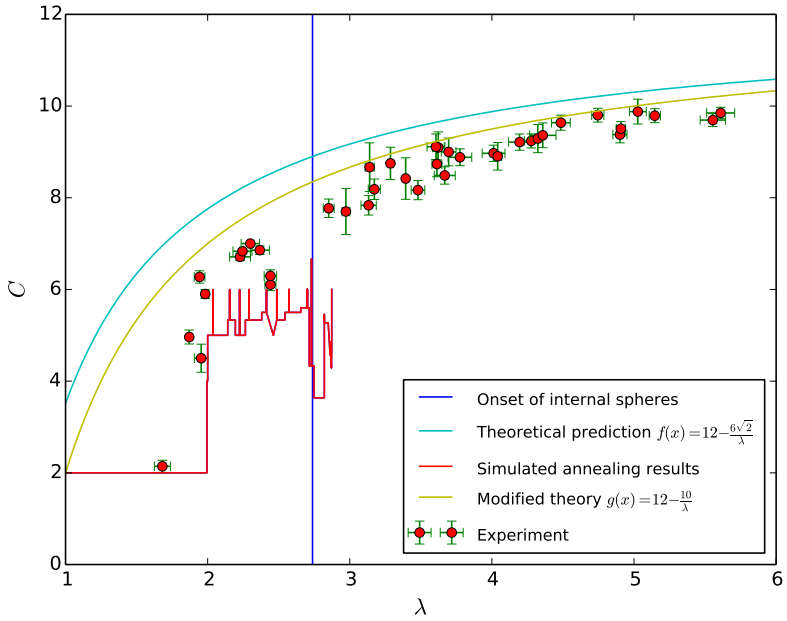

Figure 5: Variation of the average number of contacts C within the cylindrical foam structures with λ. It is seen that, as λ increases, the system approaches $C = 12$, the values associated with maximal contact number in three-dimensions. A theoretical prediction for the average contact number is shown in cyan, a fit to the experimental data in green, while the results of simulated annealing are shown in red (data taken from Mughal *et*. al. [3]).

The average contact number is seen to increase with λ. This is expected as, for the minimum $\lambda = 1$, the coordination number of the resulting linear stacking of spheres is 2. As $\lambda \to \infty$, the coordination number will approach 12, the value associated with the fcc arrangement of spheres. When compared to the results of simulated annealing (shown in red), the foam has a higher average coordination number. This is a result of the finite deformability of the bubbles of the foam allowing them to pack closer together, accessing structures with a higher average coordination number when compared to simulated annealing. We can roughly model the behaviour of our data by examining the average coordination number of spheres within an fcc lattice with a nearest neighbour separation of a.

A simple examination of the lattice shows that the density of points within this lattice ρ is given by

$$\rho = \frac{\sqrt{2}}{a^3}. \tag{2}$$

The density of *bonds* within this lattice ρ_B is given as

$$\rho_B = 3\rho = \frac{3\sqrt{2}}{a^3}. \tag{3}$$

On average, a plane, of angle ϕ and α with respect to an arbitrary normal vector $\vec{z}$, will cut N bonds per unit area where

$$\begin{aligned} N &= \sqrt{2} d \rho_B \sin(\theta) \cos(\theta) \\ &= \frac{3}{a^2}, \end{aligned}$$

where $\cos\theta$ and $\sin(\theta)$ are averaged between 0 and $\frac{\pi}{2}$. A cylinder of length l and diameter D inserted into an fcc lattice will cut N_c bonds given by

$$N_c = \frac{3\pi D l}{a^2}. \tag{4}$$

The number of bonds within this cylinder is given by

$$\frac{\pi D^2 l}{4} \rho = \frac{\pi D^2 l}{2\sqrt{2} a^3}. \tag{5}$$

The number of internal contacts of each sphere is then given as

$$\begin{aligned} C &= 12 - \frac{\text{number of cut bonds}}{\text{number of spheres}} \\ &= 12 - 6\sqrt{2}\frac{1}{\lambda}. \end{aligned}$$

Our simple model captures the expected behaviour as $C \to \infty$, however differs from what we see in experiment for lower λ value structures. For these crystals the effect of the boundary becomes more important, leading to the divergence from our model. We produced a modified theory which has the correct coordination number at low λ value - $C = 12 - \frac{10}{\lambda}$. We see that this curve, while still over-estimating the coordination number, lies closer to the experimental and theoretical results.

When compared to the results of our foam experiments and simulated annealing, the model over-estimates the number of contacts. This is due to the model's assumption that we are cutting through the closest-packed structure - the FCC lattice. For the case of the confined systems studied, the boundary will frustrate the formation of this most efficiently packed system, resulting in a lower coordination number for a given λ value.

4 Conclusions

Our experiments have shown that monodosperse wet foams confined within cylindrical channels demonstrate many of the ordering characteristics of hard-sphere column crystals. The same structures occur, at the same points, for both hard-sphere and foam structure at low λ value. This indicates that the difference in interactions between bubbles and hard-spheres does not result in a dramatic change in the structures formed. On increasing λ, beyond the current limits of simulation, structures composed of bubble shells occur. For such structures, the innermost shell resembles those structures found at lower λ values.

When the coordination number of these structures was measured, it was found that the coordination number increased with λ values in a coherent manner. The simple theory put forward indicates that the coordination number of columnar crystals increased as $\lambda = 12 - \frac{A}{\lambda}$. When compared to our data, we found that this functional form fit well with $A = 12.5$. When comparing theory to experiment and simulation, we found that both the theory and experiment over-estimate the coordination number when compared to simulation, the experiment being a closer match. This is a result of the finite compressibility of the foam resulting in more densely-packed systems. We may conclude that our foam systems are good in determining the structure of a sphere-packing for a particular λ value in a quantitative manner - more care must be taken when trying to compare qualitative measurements directly.

5 Outlook

The current accuracy of our experiments is limited by the small number of bubbles which resided within the capillary length of the liquid phase. This limitation may be overcome,however, through the use of bubbles of smaller diameter. As the bubble diameter is decreased, the bubbles will become less deformable, appearing more like hard spheres. In addition, as the number of layers of foams which reside within the capillary length is inversely proportional to the average bubble diameter of the foam, smaller bubbles will result in better statistics for our coordination number calculations. However, bubbles far below the average diameter imaged for this paper, in the range of $100\mu m$, are beyond the imaging capabilities of our current lab-based X-ray equipment.

In future we would like to extend our current experiment by imaging our foams at a synchrotron facilities e.g. at the BESSY beamline, where the required high detector sensitivity is available to image such small bubbles. In this way we hope to extend the study of these cylindrical crystals beyond the current limits of simulations, which are currently difficult to extend due to the long computational times involved.

6 Acknowledgements

This publication has emanated from research conducted with the financial support of Science Foundation Ireland (08/RFP/MTR1083). Research also supported by the European Space Agency (MAP AO-99-108:C14914/02/NL/SH and AO-99-075:C14308/00/NL/SH) and European Union MPNS COST Action MP1106. Thanks to Prof. Denis Weaire for his many helpful discussions and suggestions. Thanks to Dr. Jason Jensen and the group of Prof. Martin Hegner for the assistance in producing the various 3D printed components used in this work, and Dr. Ho-Kei Chan for several useful discussions regarding the work of this paper. Thanks to Evan Gravelle and Aisling Johnson for their work during their summer interships.

References

[1] Thomas C. Hales. A proof of the kepler conjecture. *Annals of Mathematics*, 162:1065, 2005.

[2] A. Mughal, H. K. Chan, and D. Weaire. Phyllotactic description of hard sphere packing in cylindrical channels. *Phys. Rev. Lett.*, 106:115704, 2011.

[3] A. Mughal, H. K. Chan, D. Weaire, and S. Hutzler. Dense packings of spheres in cylinders: Simulations. *Phys. Rev. E*, 85:051305, May 2012.

[4] Galen T. Pickett, Mark Gross, and Hiroko Okuyama. Spontaneous chirality in simple systems. *Phys. Rev. Lett.*, 85:3652–3655, Oct 2000.

[5] Ralph O Erickson. Tubular packing of spheres in biological fine structure. *Science*, 181(4101):705–716, 1973.

[6] D. Weaire and S. Hutzler. *The Physics of Foams*. Oxford University Press, Oxford, 1999.

[7] A.J. Meagher, D. McAteer, S. Hutzler, and D. Weaire. Building the pyramids: perfect bubble crystals. *Philosophical Magazine*, 93(31-33):4138–4150, 2013.

[8] A. M. Ganan-Calvo. Perfectly monodisperse microbubbling by capillary flow focusing: An alternate physical description and universal scaling. *Physical Review E*, 69(2), 2004. Part 2 027301.

[9] A. van der Net, W. Drenckhan, D. Weaire, and S. Hutzler. The crystal structure of bubbles in the wet foam limit. *Soft Matter*, 2(2):129–134, 2006.

[10] C. S. Smith. On blowing bubbles for braggs dynamic crystal model. *Journal of Applied Physics*, 20(6):631–631, 1949.

[11] R. Höhler, Y. Y. C. Sang, E. Lorenceau, and S. Cohen-Addad. Osmotic pressure and structures of monodisperse ordered foam. *Langmuir*, 24:418–425, 2008.

[12] D. Weaire and V. Pageron. Frustrated froth: Evolution of foam inhibited by an insoluble gaseous component. *Philos. Mag. Lett.*, 62:417 – 421, 1990.

[13] M Dierick, B Masschaele, and L Van Hoorebeke. Octopus, a fast and user-friendly tomographic reconstruction package developed in labview. *Measurement Science and Technology*, 15(7):1366, 2004.

[14] Mavi - modular algorithms for volume images. http://www.itwm.fraunhofer.de/en/departments/image-processing.

[15] Povray - the persistance of vision raytracer. http://povray.org.

[16] S. T. Tobin, J. D. Barry, A. J. Meagher, B. Bulfin, C. E. O'Rathaille, and S. Hutzler. Ordered polyhedral foams in tubes with circular, triangular and square cross-section. *Colloids and Surfaces A: Physicochemical and Engineering Aspects*, 382(1-3):24–31, 2011.